ATLAS NOTE

ATLAS-CONF-2012-088

July 1, 2012

Search for New Phenomena in the Dijet Mass Distribution using 5.8 fb^{-1} of pp Collisions at $\sqrt{s} = 8$ TeV collected by the ATLAS Detector

The ATLAS Collaboration

Abstract

The invariant mass distribution of dijets produced in LHC proton-proton collisions at a center-of-mass energy of $\sqrt{s} = 8$ TeV has been studied with the ATLAS detector using 2012 data with an integrated luminosity of 5.8 fb^{-1}, including dijet masses up to ~ 4.1 TeV. No resonance-like features have been observed. A new ATLAS limit excludes excited quarks with masses below 3.66 TeV at 95% C.L. Model-independent limits on the product of production cross-section and acceptance $\sigma \times \mathcal{A}$ have also been extended.

ATLAS-CONF-2012-088
07 July 2012

1 Introduction

At the CERN Large Hadron Collider (LHC), collisions with the largest momentum transfer typically result in final states featuring two high transverse momentum (p_T) jets of particles. The study of these two-jet (dijet) events provides an opportunity to test the Standard Model (SM) at the highest energies accessible to the LHC. At these energies, new particles could be produced [1,2], new interactions between particles could manifest themselves [3–6], or forces like gravity [7–12] could become strong. These collisions also probe the structure of the fundamental constituents of matter at the smallest distance scales, allowing for example an experimental test of the size of quarks, which are treated in the SM as point-like particles [13–15].

In 2012, the center-of-mass (CM) energy for proton-proton (pp) collisions at the LHC was raised from 7 TeV to 8 TeV. The current study focuses on the highest p_T dijet events from pp collision data accumulated by the ATLAS detector [16] since the start of 8 TeV running, corresponding to an integrated luminosity of 5.8 fb^{-1}.

As in previous analyses [17–23] the method employed to search for new phenomena (NP) is to look for localised excesses in the dijet mass (m_{jj}) distribution (often referred to as "bumps" or "resonances"). No resonances associated with new phenomena have been found in previous studies.

An essential element of the search method is to apply kinematic selection criteria that retain the highest p_T collisions and which also emphasise the angular regions where new phenomena are expected to appear. The two jets emerging from the collision are reconstructed to determine m_{jj} and the scattering angle in the dijet CM. The dominant Quantum Chromodynamics (QCD) interaction in this high-p_{T} scattering regime involves t-channel processes, leading to angular distributions that peak at small scattering angles. In contrast, most NP models predict that the angular distribution of the NP signal will be more isotropic than that of QCD. Angular kinematic criteria are used to select large angle scattering events, emphasising the central scattering region where NP processes would be expected to appear.

One important consequence of the increase in LHC energy from 7 TeV to 8 TeV is the raising of the kinematic limit by 1 TeV, which translates almost directly into a 1 TeV increase in the upper limit of accessible m_{jj}. However, a much greater increase in the sensitivity to new phenomena comes from another effect, the increase in parton luminosity as a function of $\sqrt{\hat{s}}$, the energy in the two-parton CM. The parton luminosity rises with beam energy for $\sqrt{\hat{s}}$ greater than 1 TeV [24], and at the highest dijet masses $\sqrt{\hat{s}}$ is roughly equivalent to m_{jj}. The net effect is that a data sample taken at 8 TeV with a given pp integrated luminosity will have larger sensitivity to NP processes than a 7 TeV data sample of the same integrated luminosity.

The current study uses two NP benchmarks employed in previous studies: excited quarks (q^*) [1, 2], and a model-independent resonance search based on a Gaussian mass template [23]. The CMS Collaboration has published a dijet resonance search using 1.0 fb^{-1} of 2011 data excluding excited quarks below 2.49 TeV, along with other limits [21]. The most recent preliminary result from the ATLAS experiment [25], based on 4.8 fb^{-1} of 2011 data, excludes excited quarks below 3.35 TeV (with an expected limit of 3.09 TeV).

2 The ATLAS detector and dijet kinematic variables

A detailed description of the ATLAS detector has been published previously [16]. The detector is instrumented over almost the entire solid angle around the pp collision point with layers of tracking detectors, calorimeters, and muon chambers.

High transverse momentum hadronic jets in the analysis are measured using a finely segmented calorimeter system, designed to achieve a high reconstruction efficiency and an excellent energy resolution. The electromagnetic calorimetry is provided by high granularity liquid argon (LAr) sampling calorimeters using lead as an absorber that are split into barrel ($|\eta| < 1.475$) and end-cap ($1.375 < |\eta| < 3.2$) regions. The hadronic calorimeter is divided into barrel and extended barrel ($|\eta| < 1.7$) and

Hadronic End-Cap (HEC; $1.5 < |\eta| < 3.2$). The barrel and extended barrel are instrumented with tile scintillator/steel, while the HEC uses LAr/copper calorimeter modules. The Forward Calorimeter region (FCal; $3.1 < |\eta| < 4.9$) is instrumented with LAr/copper and LAr/tungsten modules to provide electromagnetic and hadronic energy measurements, respectively.

The online event selection is performed using the ATLAS three-level trigger system, with the first level trigger (L1) being custom-built hardware and the two higher level triggers (HLT) being realised in software on large computer clusters.

As noted above, the kinematic criteria used to select events of interest for the current study involve both energy and angle variables. The dijet invariant mass, m_{jj}, is calculated from the vectorial sum of the four-momenta of the two highest p_{T} [1] jets in the event. The angular distribution for $2 \rightarrow 2$ parton scattering is predicted by QCD in the CM frame of the colliding partons, which is Lorentz boosted along the beamline due to the differing momentum fractions (Bjorken x) of the colliding partons. Relating this to jets observed in the detector, it is useful to define the jet rapidity $y \equiv \frac{1}{2}\ln(\frac{E+p_z}{E-p_z})$, where E is the jet energy and p_z is the z-component of the jet's momentum. In a given event, the rapidities in the pp system of the two highest p_{T} jets are denoted by y_1 and y_2, and the rapidities of the jets in their CM frame are $y^* = \pm\frac{1}{2}(y_1 - y_2)$. The longitudinal motion of the dijet CM system in the pp CM frame is described by the rapidity boost, $y_B = \frac{1}{2}(y_1 + y_2)$.

3 Jet calibration

Jets are reconstructed using the anti-k_t jet clustering algorithm [26, 27] with the distance parameter, R, of 0.6. The jet calibration procedure described in this section accounts for the shift in the jet response caused by the presence of multiple events in each bunch crossing, and it restores the corrected jets to the hadronic energy scale [28].

During the ATLAS 2012 data taking period the LHC instantaneous luminosity has risen substantially with respect to 2011. The mean number of inelastic interactions per bunch crossing, μ, is measured by the ATLAS luminosity detectors [29, 30] in sampling intervals of approximately one minute, and it has risen above 30 for the runs with highest instantaneous luminosity. A specific jet energy scale correction is applied to account for the effects on the jet response from additional interactions within the same bunch crossing ("in-time pileup") and from interactions in bunch crossings preceding or following the one of interest ("out-of-time pileup"). The jet response is affected by out-of-time pileup as the electronic shaping time of the liquid argon calorimeters is longer than the bunch spacing. The jet energy is adjusted by an "offset", specific to the jet algorithm and dependent on the average pileup conditions for the event. The pileup offset correction is derived from Monte Carlo samples of QCD jets (described in detail in Section 6), and validated with *in situ* studies. It restores the calorimeter energy scale, on average, to a reference point where pileup is not present. Finally, jets are calibrated to the hadronic scale using constants that are functions of the jet p_{T} and pseudorapidity. The calibration constants are derived from the Monte Carlo (MC) simulation of jet events, and they have been validated with extensive studies using test-beam and collision data.

An initial estimate of the jet energy scale uncertainty has been derived using the 2010 estimate as a baseline [28], augmented with flavor and topology uncertainties from 2011 studies. The uncertainty on the absolute scale of the calibration has been derived from Monte Carlo studies on the nominal QCD simulation sample, with event generator tunes and PDFs detailed further in Section 6. A p_{T} and η dependent jet energy scale uncertainty as low as 4% in the central detector region is assigned to calibrated jets. The uncertainty has been extended to the forward region employing η intercalibration studies in

[1] In the right-handed ATLAS coordinate system, the pseudorapidity η is defined as $\eta \equiv$ -ln tan(θ/2), where the polar angle θ is measured with respect to the LHC beamline. The azimuthal angle ϕ is measured with respect to the x-axis, which points toward the center of the LHC ring. The z-axis is parallel to the anti-clockwise beam viewed from above. Transverse momentum and energy are defined as $p_T = p\sin\theta$ and $E_T = E\sin\theta$, respectively.

dijet events, performed in 2011. The 2011 estimate of the pileup uncertainty [31] has been validated with *in situ* momentum balance techniques in studies of 2012 data, and it produces an additional source of systematic uncertainty depending on the number of primary vertices, and on μ.

4 Event triggers and selection criteria

The logical OR of two central ($|\eta| < 3.2$), single-jet triggers is used to select events having at least one large transverse energy deposition in the calorimeter. The first trigger employs all three trigger levels of ATLAS, selecting jets above a threshold of 360 GeV using jet definitions and calibration close to offline reconstruction for jets with the distance parameter R=0.4. The second trigger is a first (hardware)-level trigger with a threshold at 350 GeV on the raw calorimeter energy of the jets. Used in OR with the first trigger, it avoids inefficiencies due to splitting and merging of jets that could arise from the use of the distance parameter R=0.6 in the analysis. The kinematic selection criteria employed in the current study assure that this trigger combination is used on the trigger efficiency plateau (efficiency greater than 99%) to avoid the need for corrections.

Events are required to have a primary collision vertex defined by two or more charged particle tracks. There must be at least two jets in the event. A jet-by-jet correction is applied to account for temporary malfunctioning of some Tile calorimeter cells. Beam background jets are subsequently rejected. At this point, the highest-p_{T} jet is referred to as the "leading" jet, the second-highest-p_{T} as the "subleading" jet; the dijet invariant mass m_{jj} is calculated from these two jets.

In order to maximise the sensitivity to new phenomena manifesting as two central jets, only events with both leading and subleading jets within $|y| < 2.8$ are retained. Fake jet rejection criteria are described in detail in Reference [32]. Events are rejected if there is evidence of either noise bursts or data corruption in the data from the liquid argon calorimeter. There must be no poorly measured jets with p_{T} greater than 30% of the p_{T} of the subleading jet. These criteria also require that, if either of the leading jets is not attributed to in-time energy depositions in the calorimeters, the event is to be rejected. Events are also rejected if either the leading or subleading jet contains anomalous energy deposits, such as those resulting from overactive cells in a region of the calorimeter that was problematic for some period of data taking. All data corruption and jet quality criteria taken together reject less than 1.1% of the events.

Further kinematic selection criteria are used to enrich the sample with events in the hard-scattering region of phase space. In addition to the $|y_{1,2}| < 2.8$ criterion described above, events must satisfy $|y^*| < 0.6$ and $m_{jj} > 1000$ GeV. The final dijet mass distribution from collision data is not corrected (unfolded) for detector resolution effects.

The combination of kinematics and trigger selection restricts jets in the analysis to have a minimum p_T of 150 GeV. The maximum jet p_T observed is 2.1 TeV, contributing to the highest invariant mass event of 4.1 TeV.

5 Comparing the dijet mass spectrum to a smooth background

In the dijet mass analysis, the m_{jj} spectrum is searched for resonances by employing a data-driven background estimate that does not rely on QCD calculations. The observed dijet mass distribution after all selection cuts is shown in Fig. 1. As in previous dijet resonance analyses, the m_{jj} spectrum is fitted to a smooth functional form,

$$f(x) = p_1(1-x)^{p_2} x^{p_3+p_4 \ln x}, \tag{1}$$

where the p_i are fit parameters, and $x \equiv m_{jj}/\sqrt{s}$. In previous studies, ATLAS and other experiments [18–20, 22] have found this ansatz to provide a satisfactory fit to the QCD prediction of dijet production. The use of this smooth background form brings in the uncertainties associated with its fit parameters, but avoids the theoretical and systematic uncertainties that are encountered in the alternative approach, using a MC QCD background prediction. Another feature of the fitting form is that it allows for smooth background variations, but does not accommodate localised excesses that could indicate the presence of

NP signals. However, the effects of smooth deviations from QCD, such as those associated with contact interactions, could be partially compensated by the background fitting function, and therefore, the m_{jj} analysis is used only to search for resonant effects.

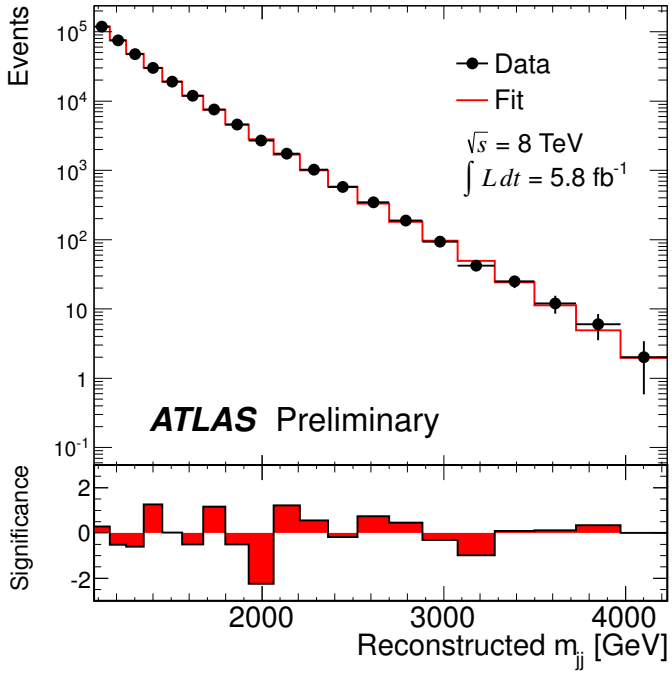

Figure 1: The reconstructed dijet mass distribution with statistical uncertainties (filled points with error bars) fitted with a smooth functional form (solid line). The bin-by-bin significance of the data-fit difference is shown in the lower panel, using positive values for excesses and negative values for deficits. If a p-value greater than 50% is found the corresponding significance is not shown (see text).

The χ^2 value of the fit is 13.8 for 16 DF. The lower panel of Fig. 1 shows the significance, in standard deviations, of the difference between the data and the fit in each bin. The significance is purely statistical, and based on Poisson distributions. The contents of a given bin are used to determine the p-value, the probability of the background fluctuating higher than the observed excess or lower than the observed deficit. The p-value is transformed into a significance in terms of an equivalent number of standard deviations (the z-value) [33]. Where there is an excess (deficit) in data in a given bin, the significance is plotted as positive (negative). In certain cases, individual bins are not plotted. [2]

To determine the degree of consistency between data and the fitted background, the p-value of the fit is obtained by calculating the χ^2 value from the data, and comparing this result to the χ^2 distribution obtained from pseudoexperiments, as described in a previous publication [22]. The resulting p-value is 0.38, showing that there is reasonable agreement between the data and the functional form.

As a more sensitive test, the BumpHunter algorithm [34, 35] is used to establish the presence or absence of a resonance in the dijet mass spectrum, as described in greater detail in previous ATLAS publications [22, 23]. Starting with a two-bin window, the algorithm increases the signal window and shifts its location until all possible bin ranges, up to half the mass range spanned by the data, have been

[2] In mass bins with a small expected number of events, where the observed number of events is similar to the expectation, the Poisson probability of a fluctuation at least as high (low) as the observed excess (deficit) can be greater than 50%, as a result of the asymmetry of the Poisson distribution. Since these bins have too few events for the significance to be meaningful, the bars are not drawn for them.

tested. The most significant departure from the smooth spectrum ("bump") is defined by the set of bins that has the smallest probability of arising from a background fluctuation assuming Poisson statistics.

The BumpHunter algorithm accounts for the so-called "look elsewhere effect" [36], by performing a series of pseudoexperiments to determine the probability that random fluctuations in the background-only hypothesis would create an excess anywhere else in the spectrum as significant as the one observed. Variable width binning reduces the penalty due to this effect, while retaining sensitivity. Furthermore, to prevent any NP signal from biasing the background estimate, if the biggest local excess from the background fit has a p-value smaller than 0.01, this region is excluded and a new background fit is performed. No such exclusion is needed for this data set.

The BumpHunter algorithm has not identified any significant discrepancy in the observed dijet mass distribution in Fig. 1. The test has a p-value for the null hypothesis (compatibility with the fit function) of 0.75 for the most discrepant set of bins, and therefore shows no evidence for a resonance signal in the m_{jj} spectrum.

6 Limits on excited quark production

In the absence of any significant signal indicating the presence of phenomena beyond QCD, the current study focuses on setting 95% credibility level (C.L.) limits on new phenomena. One NP baseline model has been chosen for analysis: the excited quark hypothesis, (q^*), used in all previous ATLAS analyses [1, 2]. This model is available in the Pythia 6 [37] and Pythia 8 [38] event generators.

For analyses up through the 2011 data set, q^* has been simulated in ATLAS using Pythia 6. Beginning with the 2012 data analysis, most ATLAS Pythia based simulations will be done with the Pythia 8 event generator. For the current q^* studies, MC samples at 8 TeV have been generated for a set of discrete q^* masses ranging from 1000 to 4000 GeV with Pythia 8 using the MC12 AU2 tune [39] with CT10 PDF's [40].

To allow for comparison with Pythia 8, MC samples at 8 TeV have also been generated with Pythia 6, using the MC11 AUET2B tune [41] and CT10 PDF's. These studies show that the dijet mass peak is substantially wider in Pythia 8 than in Pythia 6. The Pythia authors have identified a long-standing misapplication of QCD final state radiation (FSR) vetoing in Pythia 6, which is resolved in the Pythia 8 model used for the current study. The widening of the peak in Pythia 8 affects the search sensitivity and exclusion limits, including those quoted in the analysis of the 2011 dataset [25]. In this note the Pythia 8 exclusion limit is the reported result, and the Pythia 6 limit is listed for comparison.

In the current studies, the Bayesian method documented in [22] is applied to data for each considered mass of the q^*, to set a 95% C.L. limit on $\sigma \times \mathcal{A}$ for an NP signal as a function of m_{q^*}, using a prior probability distribution constant in signal strength. The limit on m_{q^*} is then determined by comparing the resulting set of limits on $\sigma \times \mathcal{A}$ from data with the corresponding values predicted from the set of theoretical samples simulated using Pythia 8. This form of analysis is applicable to resonant phenomena where the NP couplings are strong at the signal mass and interference with QCD terms can thus be neglected.

The acceptance calculation based on the MC samples includes all MC reconstruction steps and analysis cuts described in Section 4. For q^*, the acceptance $\mathcal{A}$ ranges from 11% to 54% for m_{q^*} varying from 1 TeV to 4.25 TeV, and is never lower than 48% for masses above 2 TeV. The main impact on the acceptance comes from the rapidity selection criteria.

The resulting limits are illustrated in Fig. 2. As described above, the observed limit curve is derived from data in each m_{jj} mass bin using pseudoexperiments. The expected limit curve is found from pseudoexperiments assuming background only. The dashed theoretical curve for q^* is derived from the Pythia 8 MC samples, and the points where this curve crosses the first two curves determine the observed and expected limits in terms of m_{q^*}. The expected lower mass limit at 95% C.L. for q^* is 3.53 TeV, and the observed limit is 3.66 TeV. The 1 and 2 σ uncertainty bands in Fig. 2 include the effects of systematic

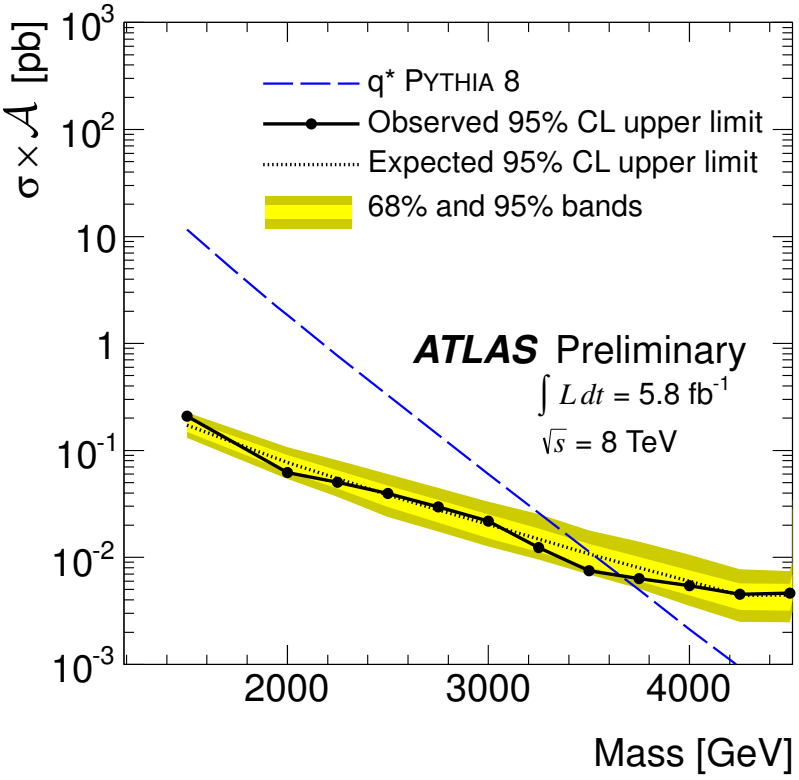

Figure 2: The 95% C.L. upper limits on $\sigma \times \mathcal{A}$ (where $\mathcal{A}$ denotes the acceptance) as a function of particle mass reconstructed using using m_{jj} (black filled circles). The black dotted curve shows the 95% C.L. upper limit expected from Monte Carlo and the light and dark yellow shaded bands represent the 68% and 95% contours of the expected limit, respectively. Theoretical predictions of $\sigma \times \mathcal{A}$ are shown for excited quarks (dashed). The observed (expected) limit occurs at the crossing of its $\sigma \times \mathcal{A}$ curve with the observed (expected) 95% C.L. upper limit curve.

uncertainties due to luminosity, acceptance, background parameterisation and jet energy scale. These uncertainties are incorporated into the fit by varying all sources according to Gaussian probability distributions and convolving them with the Bayesian posterior probability distribution. Credibility intervals are then calculated numerically from the resulting convolutions.

The luminosity uncertainty for the 2012 data is 3.6%, and is combined in quadrature with the acceptance uncertainty. The background parameterisation uncertainty is derived from the fit results, as explained in [22]. The JES uncertainty, discussed in Section 3, shifts resonance mass peaks by less than 4%. The effect of the jet energy resolution uncertainty is found to be negligible.

No uncertainties are associated with the theoretical model, as the q^* model is a benchmark that incorporates a specific choice of model parameters, PDF set, and MC tune. Previous ATLAS studies using the q^* theoretical prediction [22] (using the PYTHIA 6 generator) showed that the variation of the limits among three different choices of MC tune and PDF set was less than 4% for the expected limits.

The exclusion limits at 95% C.L. for q^* have also been determined using the PYTHIA 6 MC samples. The expected limit is shifted to a higher q^* mass of 3.71 TeV (3.79 TeV observed). This upward shift was anticipated since the PYTHIA 6 mass distribution (lacking FSR) is narrower than that predicted by PYTHIA 8.

7 Model-independent limits on dijet resonance production

As in previous dijet resonance analyses, limits on dijet resonance production are determined here using a Gaussian resonance shape hypothesis. Limits are set for a collection of hypothetical signals that are assumed to be Gaussian-distributed in m_{jj} with mean (m_{G}) ranging from 1.0 to 4.0 TeV and with standard deviation (σ_{G}) from 7% to 15% of the mean.

Systematic uncertainties are treated using the same methods as applied in the model dependent limit setting described above. The only difference for the Gaussian analysis arises from the decay of the dijet final state not being simulated. In place of this, it is assumed that the dijet signal distribution is Gaussian in shape, and the JES is adjusted by modelling it as an uncertainty of 4% in the central value of the Gaussian signal. This approach has been validated by shifting the energy of all jets in Pythia 6 signal templates by their JES uncertainty and evaluating the relative shift of the mass peak.

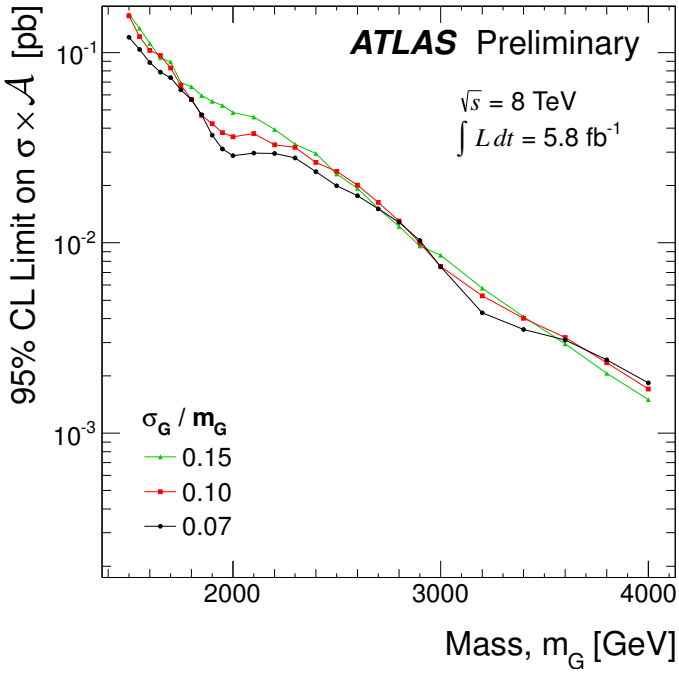

Figure 3: The 95% CL upper limits on $\sigma \times \mathcal{A}$ for a simple Gaussian resonance decaying to dijets as a function of the mean mass, m_{G}, for three values of $\sigma_{\mathrm{G}}/m_{\mathrm{G}}$, taking into account both statistical and systematic uncertainties.

The resulting limits based on 2012 data on $\sigma \times \mathcal{A}$ for the Gaussian template model are shown in Fig. 3, and the numerical contents of this figure are provided in Table 1. These results may be utilised to set limits on NP models beyond those considered in the current studies. A detailed description of the recommended procedure, including the treatment of detector resolution effects, is given in a previous publication [23].

8 Conclusions

The dijet mass distribution has been measured by the ATLAS experiment up to approximately 4.1 TeV, using 5.8 fb^{-1} of LHC pp collision data at 8 TeV. No resonance-like features have been observed in the dijet mass spectrum. A new ATLAS exclusion limit has been set for excited quarks with masses below 3.66 TeV, at 95% C.L. Model-independent limits on $\sigma \times \mathcal{A}$ have also been extended.

Table 1: The 95% CL upper limit on $\sigma \times \mathcal{A}$ [pb] for the Gaussian model. The symbols m_G and σ_G are, respectively, the mean mass and standard deviation of the Gaussian.

m_G	σ_G/m_G		
(GeV)	7%	10%	15%
1500	0.12	0.16	0.16
1550	0.10	0.12	0.13
1600	0.088	0.10	0.11
1650	0.079	0.096	0.094
1700	0.074	0.083	0.089
1750	0.064	0.067	0.069
1800	0.057	0.057	0.066
1850	0.047	0.047	0.059
1900	0.037	0.042	0.055
1950	0.031	0.038	0.053
2000	0.029	0.036	0.048
2100	0.030	0.037	0.046
2200	0.030	0.033	0.039
2300	0.028	0.032	0.033
2400	0.024	0.027	0.029
2500	0.020	0.024	0.023
2600	0.018	0.020	0.019
2700	0.015	0.016	0.015
2800	0.013	0.013	0.012
2900	0.010	0.010	0.010
3000	0.007	0.008	0.009
3200	0.004	0.005	0.006
3400	0.004	0.004	0.004
3600	0.003	0.003	0.003
3800	0.002	0.002	0.002
4000	0.002	0.002	0.002

References

[1] U. Baur, I. Hinchliffe, and D. Zeppenfeld, *Excited Quark Production at Hadron Colliders*, Int. J. Mod. Phys. **A2** (1987) 1285.

[2] U. Baur, M. Spira, and P. M. Zerwas, *Excited-Quark and -Lepton Production at Hadron Colliders*, Phys. Rev. **D42** (1990) 815.

[3] P. H. Frampton and S. L. Glashow, *Chiral Color: An alternative to the standard model*, Phys. Lett. **B190** (1987) 157.

[4] P. H. Frampton and S. L. Glashow, *Unifiable chiral color with natural Glashow-Iliopoulos-Maiani mechanism*, Phys. Rev. Lett. **58** (1987) 2168.

[5] J. Bagger, C. Schmidt, and S. King, *Axigluon production in hadronic collisions*, Phys. Rev. **D37** (1988) 1188.

[6] T. Han, I. Lewis, and Z. Liu, *Colored Resonant Signals at the LHC: Largest Rate and Simplest Topology*, JHEP **12** (2010) 085, arXiv:1010.4309 [hep-ph].

[7] P. Meade and L. Randall, *Black Holes and Quantum Gravity at the LHC*, JHEP **0805** (2008) 003, arXiv:0708.3017 [hep-ph].

[8] L. A. Anchordoqui, J. L. Feng, H. Goldberg, and A. D. Shapere, *Inelastic black hole production and large extra dimensions*, Phys. Lett. **B594** (2004) 363, arXiv:0311365 [hep-ph].

[9] S. Cullen et al., *TeV strings and collider probes of large extra dimensions*, Phys. Rev. **D62** (2000) 055012.

[10] L. Anchordoqui et al., *Jet Signals for Low Mass Strings at the Large Hadron Collider*, Phys. Rev. Lett. **100** (2008) 171603.

[11] L. Anchordoqui et al., *LHC Phenomenology for String Hunters*, Nuclear Physics **B821** (2009) 181, arXiv:0904.3547 [hep-ph].

[12] N. Kitazawa, *A closer look at string resonances in dijet events at the LHC*, JHEP **1010** (2010) 051, arXiv:1008.4989v2 [hep-ph].

[13] E. Eichten, I. Hinchliffe, K. D. Lane, and C. Quigg, *Supercollider Physics*, Rev. Mod. Phys. **56** (1984) 579.

[14] E. Eichten, I. Hinchliffe, K. D. Lane, and C. Quigg, *Erratum: Supercollider Physics*, Rev. Mod. Phys. **58** (1986) 1065.

[15] P. Chiappetta and M. Perrottet, *Possible bounds on compositeness from inclusive one jet production in large hadron colliders*, Phys. Lett. **B235** (1991) 489.

[16] ATLAS Collaboration, *The ATLAS Experiment at the CERN Large Hadron Collider*, JINST **3** (2008) S08003.

[17] UA2 Collaboration, P. Bagnaia et al., *Measurement of jet production properties at the CERN $\bar{p}p$ Collider*, Phys. Lett. **B144** (1984) 283.

[18] CDF Collaboration, T. Aaltonen et al., *Search for new particles decaying into dijets in $p\bar{p}$ collisions at $\sqrt{s} = 1.96$ TeV*, Phys. Rev. **D79** (2009) 112002, arXiv:0812.4036 [hep-ex].

[19] ATLAS Collaboration, *Search for New Particles in Two-Jet Final States in 7 TeV Proton-Proton Collisions with the ATLAS Detector at the LHC*, Phys. Rev. Lett. **105** (2010) 161801, arXiv:1008.2461 [hep-ex].

[20] CMS Collaboration, *Search for Dijet Resonances in 7 TeV pp Collisions at CMS*, Phys. Rev. Lett. **105** (2010) 211801.

[21] CMS Collaboration, *Search for resonances in the dijet mass spectrum from 7 TeV pp Collisions at CMS*, Phys. Lett. **B704** (2011) 123, arXiv:1107.4771 [hep-ex].

[22] ATLAS Collaboration, *Search for New Physics in Dijet Mass and Angular Distributions in pp Collisions at $\sqrt{s}$ = 7 TeV Measured with the ATLAS Detector*, New Journal of Physics **13** (2011) 053044, arXiv:1103.3864 [hep-ex].

[23] ATLAS Collaboration, *Search for new physics in the dijet mass distribution using 1 fb^{-1} of pp collision data at $\sqrt{s}$ = 7 TeV collected by the ATLAS detector*, Phys. Lett. **B708** (2012) 37, arXiv:1108.6311 [hep-ex].

[24] C. Quigg, *LHC Physics Potential vs. Energy: Considerations for the 2011 Run*, arXiv:1101.3201v2 [hep-ph].

[25] ATLAS Collaboration, *Search for New Phenomena in Dijet Mass and Angular Distributions using 4.8 fb^{-1} of pp Collisions at $\sqrt{s}$=7 TeV collected by the ATLAS Detector*, ATLAS-CONF-2012-038, March, 2012.

[26] M. Cacciari, G. P. Salam, and G. Soyez, *The anti-k_T jet clustering algorithm*, JHEP **04** (2008) 063, arXiv:0802.1189 [hep-ph].

[27] M. Cacciari and G. P. Salam, *Dispelling the N^3 myth for the kt jet-finder*, Phys. Lett. **B641** (2006) 57, arXiv:0512.210 [hep-ph].

[28] ATLAS Collaboration, *Jet energy measurement with the ATLAS detector in proton-proton collisions at sqrt(s) = 7 TeV*, arXiv:1112.6426 [hep-ex].

[29] ATLAS Collaboration, *Updated Luminosity Determination in pp Collisions at $\sqrt{s}$ = 7 TeV using the ATLAS Detector*, ATLAS-CONF-2011-011, March, 2011.

[30] ATLAS Collaboration, *Luminosity determination in pp collisions at $\sqrt{s}$ = 7 TeV using the ATLAS detector at the LHC*, Eur. Phys. J. **C71** (2011) 1630, arXiv:1101.2185 [hep-ex].

[31] ATLAS Collaboration, *Pile-up corrections for jets from proton-proton collisions at $\sqrt{s}$=7 TeV in ATLAS in 2011*, ATLAS-CONF-2012-064, May, 2012.

[32] ATLAS Collaboration, *Selection of jets produced in proton-proton collisions with the ATLAS detector using 2011 data*, ATLAS-CONF-2012-020, March, 2012.

[33] G. Choudalakis and D. Casadei, *Plotting the differences between data and expectation*, The European Physical Journal Plus **127** (2012) 1–11, arXiv:1111.2062v3 [physics.data-an].

[34] CDF Collaboration, T. Aaltonen et al., *Global Search for New Physics with 2.0 fb^{-1} at CDF*, Phys. Rev. **D79** (2009) 011101, arXiv:0809.3781 [hep-ex].

[35] G. Choudalakis, *On hypothesis testing, trials factor, hypertests and the BumpHunter*, arXiv:1101.0390 [physics.data-an].

[36] L. Lyons, *Open statistical issues in Particle Physics*, Ann. Appl. Stat. **2** (2008) 887.

[37] T. Sjostrand, S. Mrenna, and P. Z. Skands, *PYTHIA 6.4 Physics and Manual*, JHEP **05** (2006) 026, arXiv:0603.175 [hep-ph].

[38] T. Sjostrand, S. Mrenna, and P. Z. Skands, *A Brief Introduction to PYTHIA 8.1*, Comput. Phys. Commun. **178** (2008) 852–867, arXiv:0710.3820 [hep-ph].

[39] ATLAS Collaboration, *Further ATLAS tunes of PYTHIA6 and Pythia 8*, ATL-PHYS-PUB-2011-014, Nov, 2011.

[40] P. M. Nadolsky et al., *New parton distributions for collider physics*, Phys. Rev. **D82** (2010) 074024, arXiv:1007.2241 [hep-ph].

[41] ATLAS Collaboration, *ATLAS tunes of PYTHIA 6 and Pythia 8 for MC11*, ATL-PHYS-PUB-2011-009, Jul, 2011. https://cdsweb.cern.ch/record/1363300.

Appendices

A Comparison of signal and data with background prediction

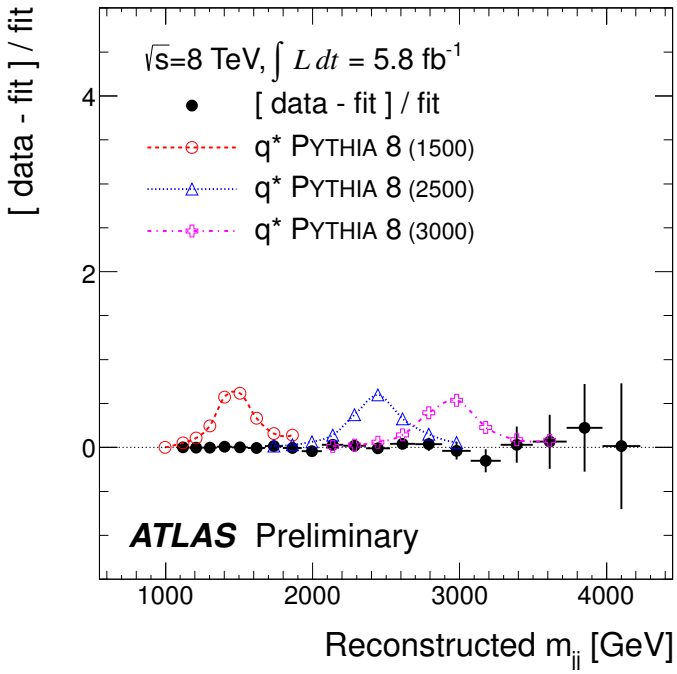

Figure 4: Three predicted excited quark (q^*) mass templates, normalised to the integrated luminosity, are compared to the data. The q^* templates and data are plotted as ratios relative to the background fit.

B Event displays of the highest dijet mass event

Figure 5 is the event display for the highest-mass dijet event entering the analysis (m_{jj}=4.1 TeV, event number 34879440, run 205113).

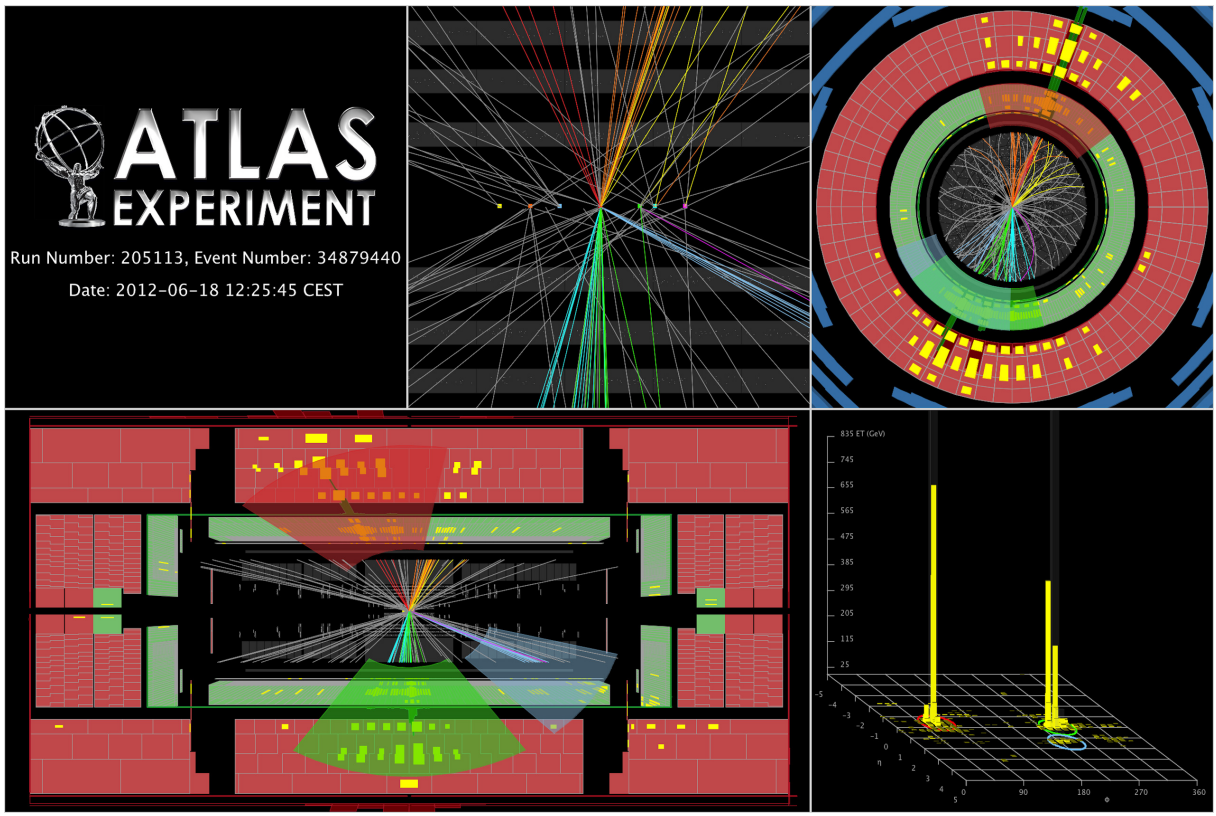

Figure 5: The highest-mass central dijet event with the highest-p_{T} jet collected by the end of June, 2012 (Event 34879440, Run 205113): the two central high-p_{T} jets have an invariant mass of 4.1 TeV, and the highest-p_{T} jet has a p_{T} of 2.1 TeV, and the subleading jet has a p_{T} of 1.9 TeV. The missing E_T and Sum E_T for this event are respectively 63 GeV and 4.2 TeV. Only tracks with $p_T > 400$ MeV are displayed. The event was collected on June 18$^{\mathrm{th}}$, 2012.